3D cellular automaton modelling of silicon crystallization including grains in twin relationship

Adrian Pineau, Gildas Guillemot, G. Reinhart, G. Regula, N. Mangelinck-Noel, Charles-André Gandin

3D cellular automaton modelling of silicon crystallization including grains in twin relationship

A Pineau[1], **G Guillemot**[1], **G Reinhart**[2], **G Regula**[2]
N Mangelinck-Noël[2] **and Ch-A Gandin**[1]

[1] MINES ParisTech, PSL Research University, CEMEF UMR CNRS 7635, CS10207, 06904 Sophia Antipolis, France
[2] Aix Marseille Univ, Université de Toulon, CNRS, IM2NP, Marseille, France

E-mail : Charles-Andre.GANDIN@mines-paristech.fr

Abstract. Production of silicon for solar cells in photovoltaic systems is mainly based on directional casting processes. Twin nucleation is favoured during silicon growth due to the low-level twin energy of formation. As a consequence, in all solidification process, a large amount of grain boundaries (GB) are in twin relationship. A 3D cellular automaton (CA) model has been recently developed for the growth of multi-crystalline silicon including facet formation and nucleation of new grains in twin relationship. Activation of facets is based on an undercooling parameter assigned to each grain and for each of the <111> crystal directions. The model also considers nucleation and growth of grains on <111> facets corresponding to Σ3 twin relationships between twin grains. This model is first applied to comparison with experimental observations. It is found that impingement of growing grains that nucleated in Σ3 twin relationships meet during growth and form Σ3, Σ9 and Σ27 GB, in good agreement with experimental observations. Finally, the model is applied at a larger scale to generate grain structures representative of industrial practice. While quantitative experimental data is missing for comparison at such scale, the model is promising and its implementation in heat and mass transfer models should be considered for assistance to production of silicon for solar cells dedicated to photovoltaic systems.

1. Introduction

Industrial photovoltaic panels are mainly based on the use of silicon material. Crystalline silicon has the largest market share due to: the availability of the raw material, non-toxicity, efficiency that could reach 15% and a high level of technology readiness [1]. The photoelectric properties of the solar cells are strongly linked to the production chain, including purity of the raw material, crystallization, wafering, cell processing, and module integration. During crystallization, the grain structure and associated defects are generated, defining density, crystallographic orientations and twin-relationships. Similarly, impurities are developed and dislocations are formed in material. The crystallization features need to be controlled in order to optimize final electrical properties because they can act as recombination centres of charge carriers, thus lowering the efficiency of the photoelectric panels [2-5].

During the manufacturing of silicon ingots in crucibles, twin grain boundaries are commonly observed in any solidification process and strongly influence the final grain structure. Voigt *et al.* [6, 7]

analysed the orientation of each grain on a 5×5 cm^2 wafer. They observed that most of the grains are in twin relationship and more than 50% of the grain boundaries correspond to Σ3, Σ9, Σ27 and Σ81 twins boundaries. The most frequent twins in silicon are of Σ3 type and can be described as an odd number of 60° rotation of the crystal lattice around a <111> direction. New grains in Σ3 relationship nucleate on {111} plane [3], their formation being enhanced by the low energy needed for twinning process [8]. According to Jackson's criterion [9], facets may correspond to the single {111} crystallographic planes in silicon material. Being coherent boundaries, Σ3 twins exhibit no dangling bonds and do not directly lower the final efficiency of solar cells [10]. However, the nucleation of a grain in Σ3 twin relationship can be at the origin of the formation of higher order incoherent, symmetric or asymmetric twin boundaries such as Σ9 or Σ27 [11] and hence responsible for part of the dislocation emission during growth [3, 12] and for impurity segregation thus degrading the photoelectric properties.

CA aims at modelling complex phenomena through the use of local simple laws. This approach was firstly proposed by Gandin and Rappaz [15] to model solidification processes. The development of grain envelopes is simulated rather than the full dendritic microstructure, with the advantage to be applicable to large simulation domains. The present work aims at modelling silicon growth upon directional solidification using a 3D CA method. The proposed model is firstly introduced. It is based on phenomenological and geometrical considerations, so as to retrieve {111} facet growth and nucleation of grains in twin relationship as commonly observed experimentally. Finally, the model is applied at a macroscopic scale to highlight the influence of facet growth and new twinned grains nucleation on the final ingot grain structure.

2. Modelling

The description of the CA algorithm is presented in [17] with details and associated schematics. The strategies implemented in the CA model to allow modelling of polycrystalline silicon growth are here briefly summarized. The model used in the present work is divided into three steps: (i) {111} facet activation and growth, (ii) grain in twin relationship nucleation and (iii) twin growth. In the following subsections, index μ refers to a liquid cell.

2.1. Facet activation and growth

The standard growth algorithm developed for cubic materials is used [17]. However, dedicated developments are introduced to model faceted growth.

2.1.1. Facet activation. Eight facets are defined for each grain, g, and tracked with virtual planes using Cartesian equations $D_g^{\{111\}}: a_g^{\{111\}}x + b_g^{\{111\}}y + c_g^{\{111\}}z + d_g^{\{111\}} = 0$. An activation undercooling, $\Delta T_g^{\{111\}}$ is associated to each plane. Its value is randomly chosen using a given normal distribution law of mean value $\Delta T_{g,m}^{\{111\}}$ and standard deviation $\Delta T_{g,s}^{\{111\}}$. If a liquid cell is captured by a growing cell belonging to grain g, its undercooling ΔT_μ is computed. This undercooling is compared to the activation undercooling, $\Delta T_g^{\{111\}}$, associated to each {111} plane leading to faceted growth for grain g. Facet activation occurs if the capture undercooling is lower than the activation undercooling ($\Delta T_\mu < \Delta T_g^{\{111\}}$). This stochastic approach is necessary to reproduce the size distribution between twin grain boundaries. The mean value and standard deviation parameters are adjusted based on comparison with experimental observations.

2.1.2. Facet growth. Facets of a grain g being described by its Cartesian equations $D_g^{\{111\}}: a_g^{\{111\}}x + b_g^{\{111\}}y + c_g^{\{111\}}z + d_g^{\{111\}} = 0$, their growth is simply modeled by the time integration of the crystal growth velocity of the {111} facets $\boldsymbol{v}_c^{\{111\}}$ defined along the normal $\boldsymbol{n}^{\{111\}}$. In practice it is sufficient to update $d_g^{\{111\}}$ with time using

$$d_g^{\{111\}} = v_c^{\{111\}}\,(t - t_0) + d_{g,t_0}^{\{111\}} \quad (1)$$

where $v_c^{\{111\}}$ is taken constant following measurements available elsewhere [16]. The CA standard algorithm is modified [17] and referred as conditioned capture algorithm. This is achieved by conditioning the capture of a cell μ by a neighboring growing cell belonging to grain g considering its location with respect to the facets described by their Cartesian equations. The coordinates (x_μ, y_μ, z_μ) of the center, C_μ, of cell μ are used in the equation associated to activated facets of grain g to compute the quantity $a_g^{\{111\}}x_\mu + b_g^{\{111\}}y_\mu + c_g^{\{111\}}z_\mu + d_{g,t_0}^{\{111\}}$. The capture is considered only if a negative value is obtained and inhibited otherwise. This condition corresponds to the facet overpassing the cell center.

2.2. Nucleation of a new grain in twin relationship

Nucleation undercooling of twinned grains on {111} facets is defined at sample edges, $\Delta T_{N,T}^E$, and at grain boundary grooves, $\Delta T_{N,T}^B$ (i.e. in the bulk material) in accordance with experimental observations. Indeed twin formation upon directional solidification is only of Σ3 type and $\Delta T_{N,T}^B$ has a lower value compared with $\Delta T_{N,T}^E$ [3, 16]. Upon capture of a liquid cell μ by its neighboring growing cell ν, location of cell μ is tested to know if it is located on a sample edge or as part of the bulk. For an edge cell (respectively a bulk cell), if the test $\Delta T_\mu > \Delta T_{N,T}^E$ (respectively $\Delta T_\mu > \Delta T_{N,T}^B$), is verified, a nucleation event takes place. The Euler angles of the new grain formed in cell μ correspond to the crystallographic orientations of the capturing grain to which a Σ3 twin rotation (60°) around the normal to the capturing facet is applied.

2.3. Twins growth

Twin boundaries between grains are locked during growth [3, 16]. To maintain the twin boundary while pursuing growth of the solid-liquid interfaces, the conditioned capture algorithm is used. The twin grain boundary remains static in space and develops as a result of growth of the grains on each side of the corresponding {111} facet. Note that this is equivalent to keep a constant value for $d_{g,t_{N,T}}^{\{111\}}$ in equation (1), defined at the time $t_{N,T}$ of the grain nucleation in twin relationship. Let us consider two grains, g_1 and g_2, in twin relationship, their common twin plane is denoted $D^{\{111\}}$ and also defined by its cartesian equation. The position of the twin plane $D^{\{111\}}$ remains unchanged. For a given liquid cell μ located in the neighbourhood of $g_1$and g_2, the capture liquid the cell μ is allowed for only g_1 or g_2, depending on the spatial position of its centre with respect to $D^{\{111\}}$. If its centre is located beneath $D^{\{111\}}$, only the capture by grain g_1 will be authorized. Capture by g_2 will occur otherwise. The reader will find schematized details of the algorithm in [17].

3. Results and discussion

3.1. Comparisons with a benchmark experiment

The 3D CA model described above is applied to simulate an experiment corresponding to observations obtained by X-ray imaging [18]. This benchmark experiment is fully detailed in [17, 18]. Numerical and process parameters as well as material properties are provided in [17]. Figure 1 shows the comparison between the simulation and experimental results. Figure 1(a) is the inverse pole figure (IPF) map along the growth direction and displayed on the longitudinal section (left) simulated and (right) measured. Figure 1(b) shows the coincidence site lattice (CSL) map (left) simulated and (right) measured. The two sets of Σ3 twin relationships with a common $(1\bar{1}1)$ plane on the right-hand side (A/B type grain boundaries) and $(11\bar{1})$ plane on the left-hand side (A/C type grain boundaries) are made of grains with

various band widths. This is directly controlled by the value of the standard deviation to activate the $\{111\}$ facets, $\Delta T_{g,s}^{\{111\}}$ (see [17] for more details).

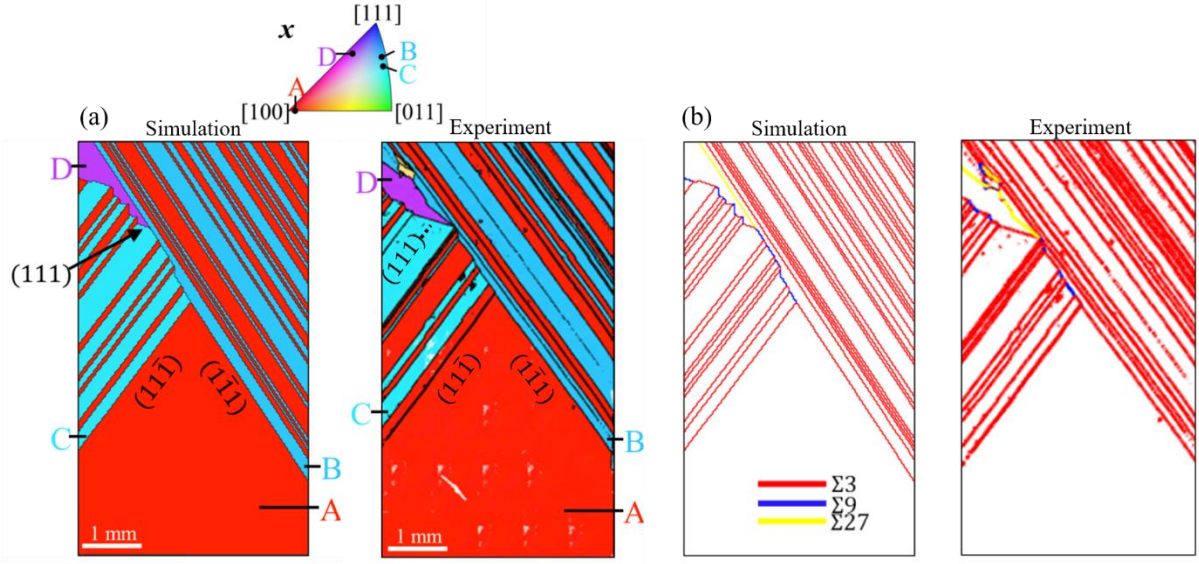

Figure 1. Qualitative comparison between the simulation results and the benchmark experiment: (a) IFP maps along the growth direction on longitudinal sections and (b) CSL maps revealing the different types of twinned GBs.

Unlike grains of B-type and C-type, the grain labelled D nucleates in the bulk at a faceted/faceted groove on a $\{111\}$ plane of a C-type grain. The Σ9 twin boundaries are observed whenever B-type and C-type or D-type and A-type grains meet, whereas a Σ27 twin boundary originates from D-type and B-type. Twin grain boundaries apart from the one due to Σ3 twin nucleation are the consequences of grain encounters during growth of A-, B-, C- and D-type grains. This result is consistent with the experimental observations. Prior to grain D nucleation, a total of 5 grooves between B-type and C-type grains were formed but did not lead to nucleation of the D-type grain on the $\{111\}$ plane of a C-type grain.

Quantitative comparisons between simulation and experiment are summarized in figure 2. The area fraction, the number of grains of types A–D and the mean twin band width of grains of type A–C were determined. For a given grain, the latter is defined by the width between two twinning events of a given grain type in a direction perpendicular to the twinning plane. The area of the initial seed is not considered when computing the grain area fraction since we focus on the grains that formed as a result of twinning nucleation events: this is why for band width computations, only edge twin nucleation is considered. One can notice the overall good agreement between simulations and experimental observations. Area fraction of A-type grains obtained in the simulation (41.3%) is very close the area fraction measured in the experiment (39.8%). The number of grains in the computation is also higher (24) than the one in the experiment (22), the mean band width being consequently a little higher, 0.11 mm in the simulation and 0.10 mm in the experiment. For B-type grains, the area fraction is 4.7% lower in the simulation (33.4%) than in the experiment (38.1%). The number of grains is almost identical and the mean band width in the simulation is lower (0.1 mm) compared to the experiment (0.12 mm). Similar observations can be done for C-type grains.

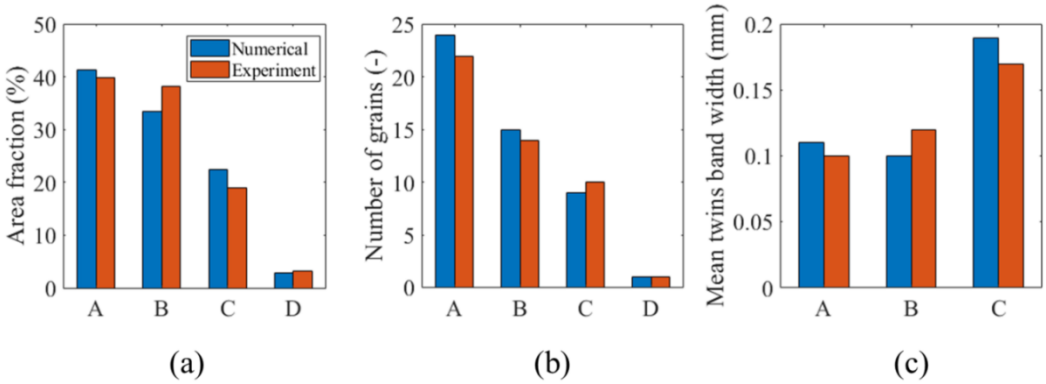

Figure 2. Statistical analyses showing (a) the area fraction, (b) the number of grains and (c) the mean band width between twin boundaries for the simulation results and the benchmark experiment shown in figure 1.

3.2. Application to a cube geometry

The model is now applied at a larger scale, *i.e.* to a cube of 5×5×5 cm^3. Three simulation cases are proposed: directional growth in an imposed and vertical temperature gradient with (i) no facet formation nor grains in twin relationship nucleation, (ii) facet formation without grains in twin relationship nucleation and (iii) facet formation and grains in twin relationship nucleation. For the sake of simplicity, these simulations are denoted I, II and III, respectively. Simulation I is similar to dendritic grain growth situation since no facet or twin nucleation are modelled in this case. The purpose of such simulations is to demonstrate the influence of the facet formation solely and facet formation coupled with twins nucleation on the final grain structure when compared to a dendritic one. In all cases, heterogeneous nucleation takes place on the bottom surface of the cube, the crystallographic orientations of the initial equiaxed grains being randomly chosen.

3.2.1. Simulation I. We firstly disable facet formation. Since twin nucleation can occur only on facets, these specific events are also disabled. The corresponding results are shown in figure 3(a). The final grain structure in displayed on the left part of figure 3(a) with a cold colour related to the misorientation, α_x, with respect to the *x* direction (growth direction). It corresponds to the lowest angle formed between all <100> crystallographic directions of the grains and the *x* axis. The centred part of figure 3(a) shows the IPF map in the *x* direction and the right one gives the CSL map. The warm colours in figure 3(a) correspond to highly misoriented grains as shown at the very beginning of the simulation at nucleation stage. The growth of highly misoriented grain is blocked in all <100> crystallographic directions. Cold colours are the only one to remain at the end of the solidification which indicates that well orientated grains, with respect to the temperature gradient, can survive. This is simply due to the grain growth competition which commonly occurs between columnar grains during directional solidification.

3.2.2. Simulation II. Facet formation is now enabled and nucleation of grains in twin relationship is disabled. The corresponding results are shown in figure 3(b). In comparison with figure 3(a), less grain remains at the end of the solidification. Regarding the misorientation, the colour code indicates that more misoriented grains survived (warm colours). This comes from the fact that some of the grains develop {111} facets and become constrained during their growth. Neighbouring grains, that grow without developing {111} facets, can solidify into the free liquid present in the facet and potentially block growth of side grains that form {111} facets.

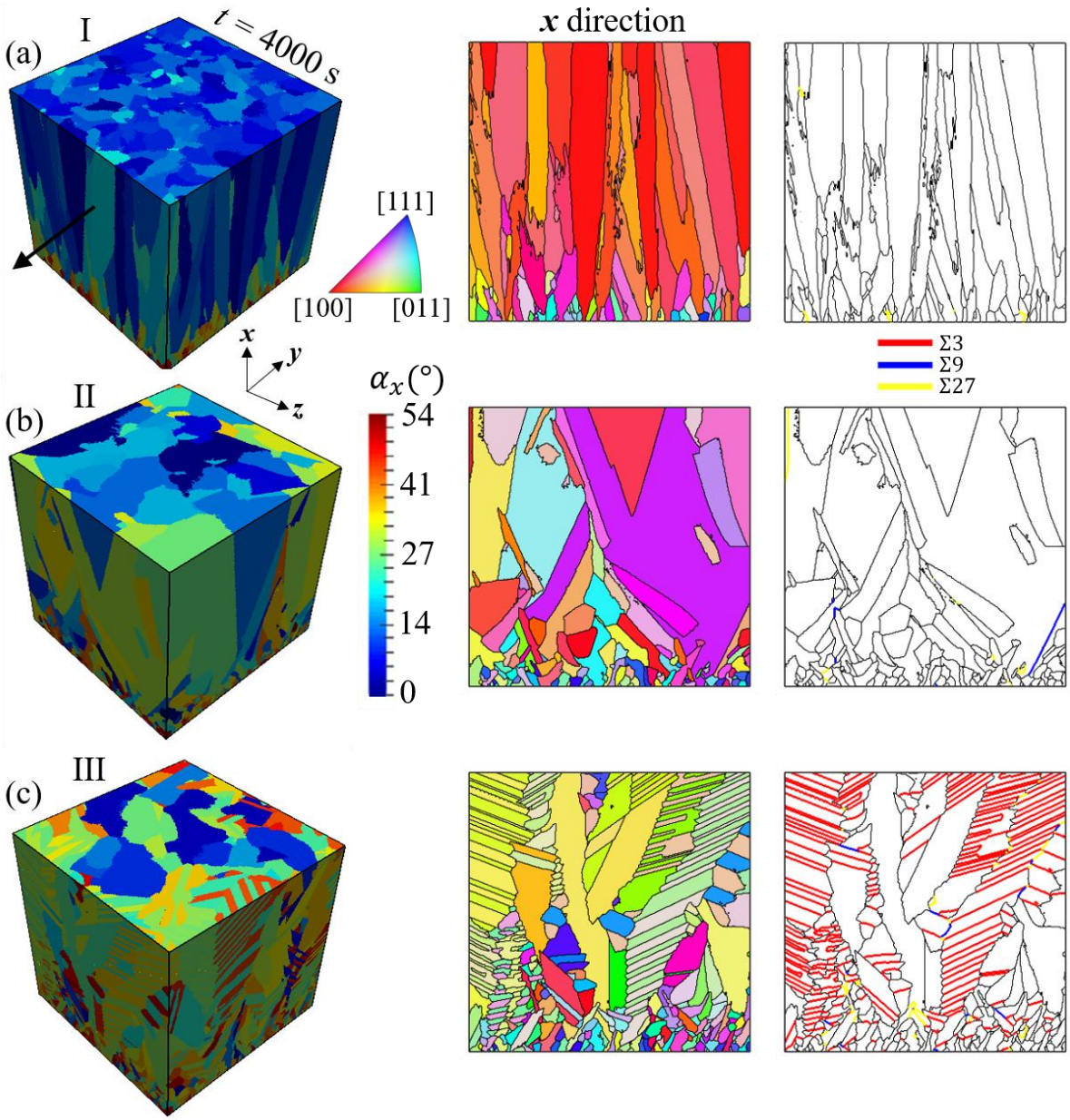

Figure 3. Results of simulations corresponding to (a) simulation I with a dendritic growth regime, (b) simulation II with growth restricted to facet formation, (c) simulation III with facet formation and grain nucleation in twin relationship. From left to right: final grain structure observed at time 4000 s showing the misorientation, α_x, the centered figure is the IFP map along the growth direction, $\boldsymbol{x}$, and the CSL map is on the right.

3.2.3. Simulation III. Both facet formation and grains in twin relationship nucleation are enabled. The corresponding results are shown in figure 3(c). Grains in twin relationship can be clearly observed in final structure. Their presence being also shown in IPF and CSL maps. As it is commonly observed in industrial casting ingots [6, 7], most of the grains are in Σ3 twin relationship. Similar explanations can be developed (figure 4) regarding the evolutions of the grain area density, n_g (figure 4(a)), and mean misorientation, $\bar{\alpha}_x$ (figure 4(b)) with respect to the solidification time, t.

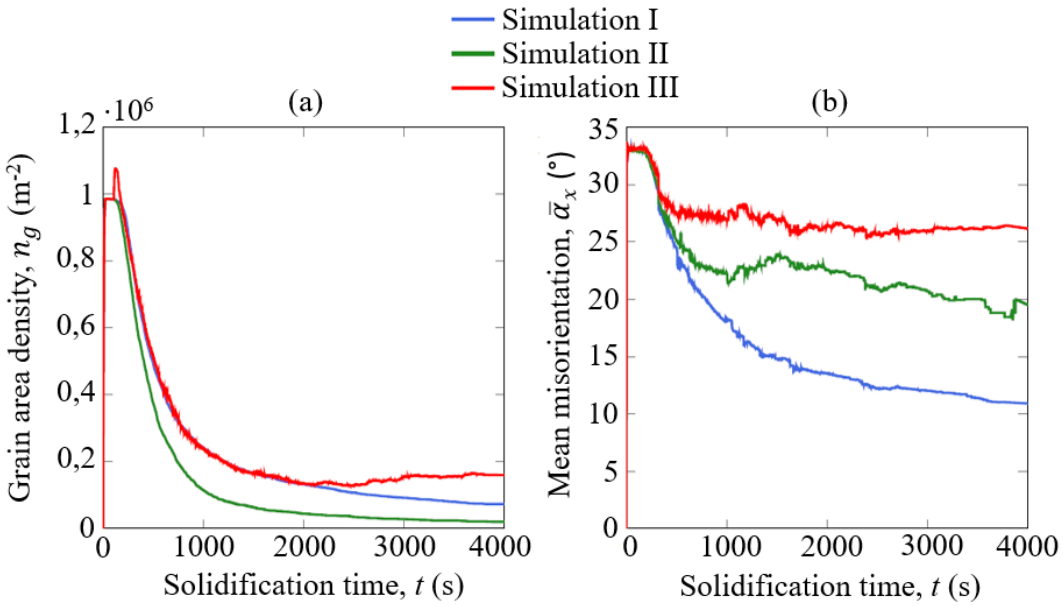

Figure 4. Evolution of (a) the grain area density, n_g, and (b) the mean misorientation, $\bar{\alpha}_x$, as a function of the solidification time, t for the three simulations cases.

For simulations I and II, the grain density n_g decreases continuously. However, the value at time $t = 4000$ s is lower in simulation II than in simulation I demonstrating that grains development is stopped due to the formation of $\{111\}$ facets on some of the grains. The value of $\bar{\alpha}_x$ at $t = 4000$ s is higher in simulation II when compared to simulation I. This is in agreement with figure 3 where more misoriented grains survive as shown in case II. Simulation III includes nucleation of grains in twin relationship. An increase in grain density at $t \approx 2600$ s is shown. It indicates that rate of twin grains nucleation overcomes grain elimination induced by grain growth competition.

4. Conclusion

A 3D CA model dedicated to the modelling of silicon solidification in multi-crystalline structure is developed. IPF and CSL maps are simulated and compared with their counterpart produced on a fully solidified sample from a benchmark experiment. Qualitative and quantitative comparisons show good agreements and similar tendencies in microstructure evolution. Application to a larger scale demonstrates that facet formation and grains in twin relationship drastically modify the final structure compared to dendritic development. Such numerical tool is suitable to follow microstructure evolution in casting process dedicated to silicon material. Future development should consequently permit grain structure optimization by direct simulation at the process scale. Further developments of the model could include a thermomechanical analysis during solidification of the grain structure, thus assessing the additional stress field that may play a role on the formation of the twin grain boundaries and of dislocations.

Acknowledgements

The present work was funded by the project CrySaLID (ANR-14-CE05-0046-01) of the French National Research Agency (ANR).

References

[1] Lacerda JS and van der Bergh JC 2016 Diversity in solar photovoltaic energy: implications for innovation and policy *Renew. Sust. Energ. Rev.* **54** 331

[2] Trempa M, Reimann C, Friedrich J, Müller G, Krause A, Sylla L and Richter T 2014 Defect formation induced by seed-joints during directional solidification of quasi-mono-crystalline silicon ingots *J. Cryst. Growth* **405** 131

[3] Tsoutsouva M G, Riberi-Béridot T, Regula G, Reinhart G, Baruchel J, Guittonneau F, Barrallier L and Mangelinck-Noël N 2016 In situ investigation of the structural defect generation and evolution during the directional solidification of ⟨110⟩ seeded growth Si *Acta Mater.* **115** 210

[4] Kakimoto K 2009 Crystallization of Silicon by a Directional Solidification Method, *Crystal Growth of Si for Solar Cells*, eds Nakajima K and Usami N (Springer Berlin Heidelberg) p 55

[5] Ouaddah H, Périchaud I, Barakel D, Palais O, Di Sabatino M, Reinhart G, Regula G and Mangelinck-Noël N 2019 Role of impurities in silicon solidification and electrical properties studied by complementary in situ and ex situ methods *Physica Status Solidi* A 1900298

[6] Voigt A, Wolf E and Strunk H P 1997 *Proc 14th Europ. PV Solar Energy Conf.* (Barcelona) p 774

[7] Voigt A, Wolf E and Strunk H P 1998 Grain orientation and grain boundaries in cast multicrystalline silicon *Mat. Sci. Eng. B* **54** 202

[8] Bristowe P D 1999 *Properties of Crystalline Si*, ed R Hull EMIS 299308

[9] Jackson K A 2004 Constitutional supercooling surface roughening *J. Cryst. Growth* **264** 519

[10] Duffar T 2010 Comprehensive review on grain and twin structures in bulk photovoltaic silicon, *Recent Res. Dev. Cryst. Growth* **5** 61

[11] Ribéri-Béridot T, Mangelinck-Noël N, Tandjaoui A, Reinhart G, Billia B, Lafford T, Baruchel J and Barralier L 2015 On the impact of twinning on the formation of the grain structure of multi-crystalline silicon for photovoltaic applications during directional solidification *J. Cryst. Growth* **418** 38

[12] Ryningen B, Stokkan G, Kivambe M, Ervik T and Lohne O 2011 Growth of dislocation clusters during directional solidification of multicrystalline silicon ingot, *Acta Mater.* **59** 7703

[13] Tandjaoui A, Mangelinck-Noël N, Reinhart G, Furter J-J, Billia B, Lafford T, Baruchel J and Guichard X 2012 Real time observation of the directional solidification of multicrystalline silicon: X-ray imaging characterization *Energy Procedia* **27** 82

[14] Tandjaoui A, Mangelinck-Noël N, Reinhart G, Billia B and Guichard X 2013 Twinning occurrence and grain competition in multi-crystalline silicon during solidification, *C. R. Physique* **14** 141

[15] Gandin Ch-A and Rappaz M 1994 A coupled finite element-cellular automaton model for the prediction of dendritic grain structures in solidification processses, *Acta Metall. Mater.* **42** 2233

[16] Stamelou V, Tsoutsouva MG, Riberi-Béridot T, Reinhart G, Regula G, Baruchel J and Mangelinck-Noël N 2017 {111} facet growth laws and grain competition during silicon crystallization *J. Cryst. Growth* **479** 1

[17] Pineau A, Guillemot G, Reinhart G, Regula G, Mangelinck-Noël N and Gandin Ch-A 2020 Cellular automaton modelling of silicon crystallization with grains in twin relationship, *Submitted for publication*

[18] Riberi-Béridot T, Tsoutsouva MG, Regula G, Reinhart G, Guittoneau G, Barrallier L and Mangelinck-Noël N 2019 Strain building and correlation with grain nucleation during silicon growth, *Acta Mater.* **177** 141